



Optimization of hydrogen production over TiO₂ supported copper and nickel oxides: effect of photoelectrochemical features

Robabeh Bashiri¹ · Norani Muti Mohamed^{1,2} · Chong Fai Kait² · Suriati Sufian³

Received: 6 July 2018 / Accepted: 18 September 2018 / Published online: 22 September 2018
© Springer Nature B.V. 2018

Abstract

Low-cost solar hydrogen production through water splitting using photo-electrochemical (PEC) cell offers a clean and renewable source of energy. However, its low performance remains a primary concern. Solar hydrogen production of TiO₂ supported copper and nickel oxides photoanode (Cu–Ni/TiO₂) was significantly influenced by photoanode fabrication and reaction parameters. To maintain the optimum operating conditions of PEC cell for practical application, we systematically investigated the effect of sintering temperature, photoanode thickness, electrolyte concentration, and applied voltage on hydrogen production over 5 mol% Cu–Ni/TiO₂ and PEC characteristics, including charge carrier transfer resistance, photocurrent density, and flat band potential. Findings reveal that the optimized sintering temperature for hydrogen production was 400 °C due to low charge transfer resistance and more excited electrons at the electrode/electrolyte interface. The photocatalyst with the four layers of printed 5 mol% Cu–Ni/TiO₂ (thickness ~ 24.8 μm) improved the photocatalytic performance, highlighting the importance of the number of excited electrons and the surface area of the photocatalyst. Furthermore, applied voltage exerted the most significant effect on hydrogen production up to 24.9 mL at the optimum level of 3.4 V by minimizing the recombination rate of electron–hole pairs. The stability of the photoanode was tested under the optimum conditions for 4 days and the maximum accumulative hydrogen of 443.4 mL was produced over this highly stable photoanode.

Electronic supplementary material The online version of this article (<https://doi.org/10.1007/s10800-018-1256-5>) contains supplementary material, which is available to authorized users.

✉ Robabeh Bashiri
robabeh.bashiri@gmail.com

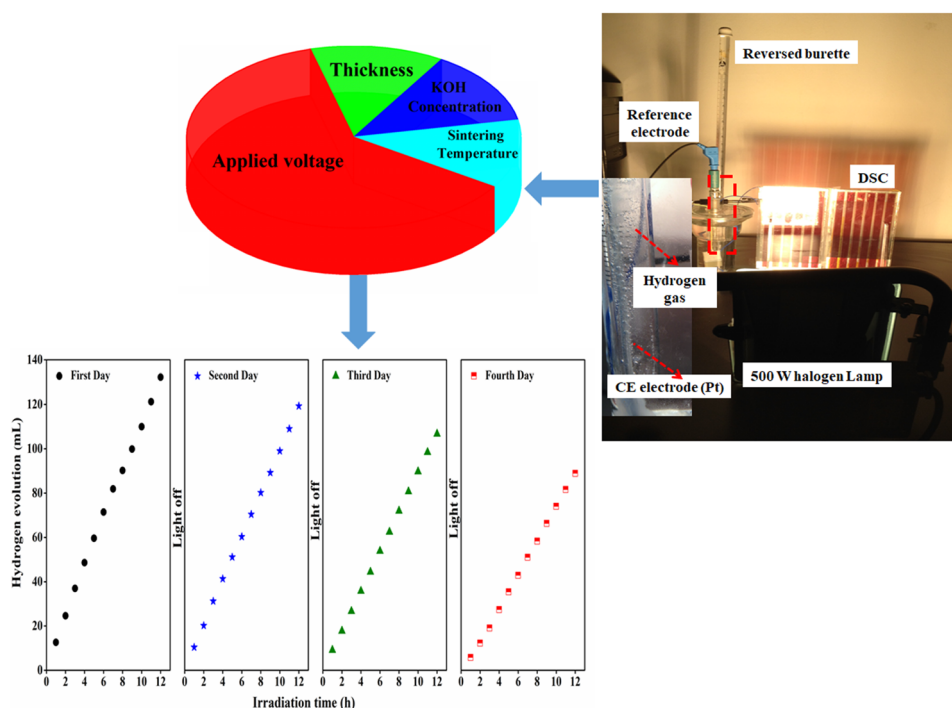
✉ Norani Muti Mohamed
noranimuti_mohamed@utp.edu.my

¹ Centre of Innovative Nanostructures & Nanodevices (COINN), Universiti Teknologi PETRONAS, 32610 Bandar Seri Iskandar, Perak, Malaysia

² Fundamental and Applied Sciences Department, Universiti Teknologi PETRONAS, 32610 Bandar Seri Iskandar, Perak, Malaysia

³ Chemical Engineering Department, Universiti Teknologi PETRONAS, 32610 Seri Iskandar, Perak, Malaysia

Graphical abstract



Keywords Photo-electrochemical cell · Sintering temperature · TiO_2 · Thin film · Electrochemical properties

1 Introduction

Obtaining clean and sustainable energy sources has become increasingly important with the extensive use of non-sustainable fossil fuels, the depletion of their reserves, and their possible environmental harm [1, 2]. Solar power is a renewable energy resource that possesses a theoretical potential of 1.2×10^5 TW, which is considerably greater than those of other renewable energy sources, such as wind, wave, hydropower and biomass [3]. Solar energy can be converted into chemical fuels, such as hydrogen fuel, through a photo-electrochemical (PEC) cell [4] as a promising alternative for carbon-based fuels, which was established by Fujishima and Honda in 1972 [5]. Photocatalytic hydrogen production is possible under ambient conditions with the use of irradiated semiconductors and mixtures of water and alcohol as electrolyte [6]. Nevertheless, the application of PEC cells is limited by their low solar energy conversion efficiency to hydrogen because no materials meet the requirements for water splitting without applying an external bias [7, 8]. Applying an additional internal or external bias is a practical approach to drive water redox reactions, overcome overvoltage losses and enhance PEC cell performance. The application of an electrical bias from fossil fuel sources or a

chemical bias based on pH differences is undesirable due to its limitations [9]. The combination of photovoltaic (PV) and PEC cells is a practical strategy to drive water redox reactions and convert solar energy into hydrogen. Dye-sensitized solar cells (DSSCs) are an attractive PV device owing to their low manufacturing cost, high photoanode stability and capacity to generate sufficient electricity for unassisted solar water splitting.

To date, visible-light active materials, such as WO_3 and Fe_2O_3 , are the main photoanodes for PEC in the PEC/DSSC system [3, 10–12]. However, these photocatalysts are mostly used for water photooxidation process due to their positive conduction band (CB) edges compared with the hydrogen redox potential [13–15]. TiO_2 is a potential candidate for PEC cell because of its unique features, including low cost, non-toxicity, water stability and negative CB position [16]. However the photocatalytic of TiO_2 -based PEC cells is still far practical approach because of their predominant absorption in the UV region, low electron mobility, and slow hole kinetics [17, 18]. Therefore, the modification of these PEC cells by shifting the absorbance edge to the visible region and diminishing the charge carrier recombination rate has the positive effect on the photocatalytic performance [19, 20]. Many research works have been reported to develop

different materials for photosplitting of water in PEC cells but less attention has been paid to the optimization of the reaction's conditions of PEC cells for photocatalytic hydrogen production in the PEC/DSSC system. Understanding the relationship between PEC/DSSC system characteristics and solar hydrogen production is important in designing an efficient solar system. In our previous study, we optimized solar hydrogen production over bimetallic Cu-/Ni-doped TiO₂ thin film in the PEC/DSSC system by varying the preparation parameters, including the molar ratios of water, acetic acid, Cu to titania precursor, calcination temperature and duration, and total metal loading [21, 22].

In the present study, we systematically investigated the effects of fabrication parameters of 5 mol% Cu–Ni/TiO₂ thin film such as sintering temperature and thickness and reaction parameters (electrolyte concentrations and applied voltages) on solar-driven hydrogen production in the PEC/DSSC system. Detailed analyses were carried out to examine the variations in charge carrier transfer resistance, photocurrent density and flat band potential in the PEC/DSSC system. Finally, the stability of the photoanode under the optimum reaction conditions was examined for continuous illumination of four days.

2 Experimental

2.1 Preparation of nanostructured 5 mol% Cu–Ni/TiO₂ photocatalysts

The 5 mol% Cu–Ni/TiO₂ photocatalyst was synthesized with sol–gel hydrothermal method using the following procedure: a solution was prepared by mixing titanium tetraisopropoxide, anhydrous ethanol, glacial acetic acid (1:8:4 ratio), Ni(NO₃)₂·6H₂O, and Cu(NO₃)₂·3H₂O (Cu:Ni:6:4 ratio with the total metal loading of 5 mol%). The prepared solution was added dropwise to a mixture of water and ethanol (32:4 ratio). The resulted hydroxide precipitates were directly transferred to a Teflon-lined stainless-steel vessel for hydrothermal treatment at 180 °C for 12 h. Finally, the products were separated and dried at 105 °C and calcined at 450 °C for 2 h. The details of the optimization processes of Cu–Ni/TiO₂ photocatalysts are reported in our previous research works [21–23].

2.2 Experimental setup and procedures

2.2.1 Fabrication of 5 mol% Cu–Ni/TiO₂ photoanode

The 5 mol% Cu–Ni/TiO₂ thin film (1 × 1 cm²) was fabricated using polyester screen material of interconnected photocatalyst particles on the surface of conductive glass (F-doped tin oxide) substrate. The details of preparation screen printable

paste are explained in our previous work [23]. A small strip of conductive silver ink as the ohmic contact was printed on the top of printed pasted and followed with sintering process and finally a copper wire was soldered on the silver strip. The prepared photoanode was immersed in a KOH solution with 5 vol% glycerol in a designed glass reactor (150 mL) for solar hydrogen measurement and photo-electrochemical study.

2.2.2 Fabrication of DSSC

The photoanode of PEC cell was connected in series to a fabricated DSSC (0.7 V), including a double-layered sensitized TiO₂ photoanode with N719 dye, a printed counter electrode with platinum paste (dyesol) and iodide/triiodide redox couple as the electrolyte. A 500 W halogen lamp was utilized as a light source for visible-light radiation ($\lambda > 400$ nm) with a light intensity of 100 mW cm⁻². The produced hydrogen was collected around the Pt rod in a reversed burette during 2 h and the gaseous products were identified by using multiple gas analyzer (SRI Instruments 8610-0071).

2.2.3 Photo-electrochemical measurements

The photo-electrochemical characteristics were studied with a conventional three-electrode configuration using a computer-controlled potentiostat (Autolab PGSTAT302N, Metrohm) with frequency response analyzer (FRA) module and NOVA software version 1.10.1.9. Electrochemical impedance spectroscopy (EIS) measurement was performed in the range of 0.1 Hz–100 kHz and AC amplitude of 10 mV in the dark using Z-Plot/Z-View to control instrument operation and data acquisition. Mott–Schottky (M–S) data were collected in the dark at a frequency of 1.0 kHz and a signal amplitude of 10 mV [24, 25]. The extrapolation on the X-axis of the M–S plot shows the flat band potential (V_{fb}). Donor density (N_D) can be calculated from the slope (m) of the linear region of the M–S plot by Eq. (1)

$$N_D = 2/\bar{e}\epsilon_0\epsilon m \quad (1)$$

where \bar{e} is an electronic charge unit (1.6×10^{-19} C), ϵ_0 is the permittivity of the free space charges (8.86×10^{-12} Fm⁻¹), ϵ is the dielectric constant of anatase TiO₂ (48 Fm) [26, 27]. The photocurrent density versus applied potential (I–V) was measured with linear sweep voltammetry (LSV) procedure for data acquisition at potential from –0.5 to 1.0 V versus Ag/AgCl with a scan rate of 20 mV s⁻¹ [21–23].

3 Results and discussion

3.1 Photocatalyst characterization

Physicochemical characteristics of the powder form of 5 mol% Cu–Ni doped TiO_2 have been described in our previous publication [21]. Briefly, photocatalyst consists of anatase nanocrystals with the average crystal sizes of 11.37 nm and its particles are almost spherical shape with average size of 11.54 nm. In addition, it had the active surface area of $76.41 \text{ m}^2 \text{ g}^{-1}$ with a band gap energy of 2.48 eV, which is capable of harvesting photons in the visible region of the solar spectrum. We reported that the accumulative hydrogen over this photocatalyst was more than other amounts of total metal loadings (10 and 15 mol%) [21]. In the following sections, the influence of sintering temperatures, photoanode thicknesses, electrolyte concentrations, applied voltages on the photo-electrochemical properties, and photocatalytic hydrogen production of 5 mol% Cu–Ni doped TiO_2 thin film are discussed in details.

3.2 Effect of sintering temperature

Photoanode paste compositions are compacted by sintering, allowing injected electrons to be collected at the underlying conductive substrate. Therefore, sintering temperature optimization is desirable to ensure good adherence of the photoanode on the substrate, eliminating the existence of organic residues in the paste and improving the connection for efficient charge transport among the nanocrystallites constituting the thin film. Figure 1a shows the thermal decomposition of the paste components and the photoanode before and after sintering. It reveals that all organic compounds were decomposed until 400 °C and the thin film showed thermal stability. Figure 1b displays that the photoanode sintered at 400 °C produced the highest accumulative hydrogen (7.8 mL) and the amount of produced hydrogen was reduced by increasing the sintering temperature. The effect of different sintering temperatures on the XRD pattern (supplementary information, Fig. S1) of 5 mol% Cu–Ni/ TiO_2 photoanode depicts that anatase TiO_2 (JCPDS 21-1272) was not affected by the sintering temperature. Increasing sintering temperature slightly shifted TiO_2 anatase peaks to a high 2θ degree without phase transition from anatase to rutile. However, the calculated crystallite sizes increase from 11.19 (400 °C) to 12.97 (500 °C) [22]. The FESEM images (Fig. S2) indicate that the increasing sintering temperature led to increase the degree of agglomeration particle sizes and reduce the porosity of the photoanode.

EIS measurements were conducted for each photo-electrode at the open circuit potential to monitor the

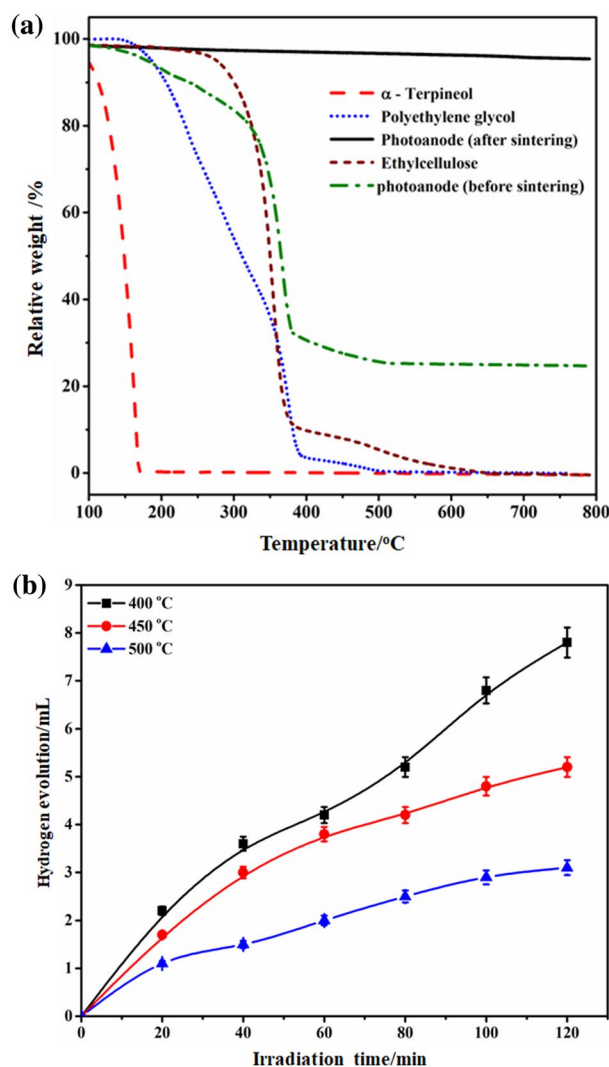


Fig. 1 **a** Thermal decomposition of paste components and photoanode before and after sintering and **b** hydrogen production at different sintering temperatures (four layers printed 5 mol% Cu–Ni/ TiO_2 , electrolyte: 1 M KOH and 5 vol%, T: 25 °C)

interaction between the electrode and electrolyte interface and charge transfer resistances. Figure 2a illustrates the typical Nyquist plots of all sintered thin films by denoting the x- and y-axis to the real part of the measured impedance (Z') and the negative number of imaginary part of the measured impedance ($-Z''$), respectively. The circuit equivalent fittings of the EIS data are presented in Table 1.

The impedance spectra demonstrated that the charge transfer resistance (R_{ct}) increased and the electron life-time significantly reduced after increasing the sintering temperature up to 500 °C. Increasing charge transfer resistance shows that the presence of several surface states can trap the electron during the EIS measurement. These trapped electrons are difficult to transfer to the interface photoanode and electrolyte [28]. Increasing the R_{ct} value beyond

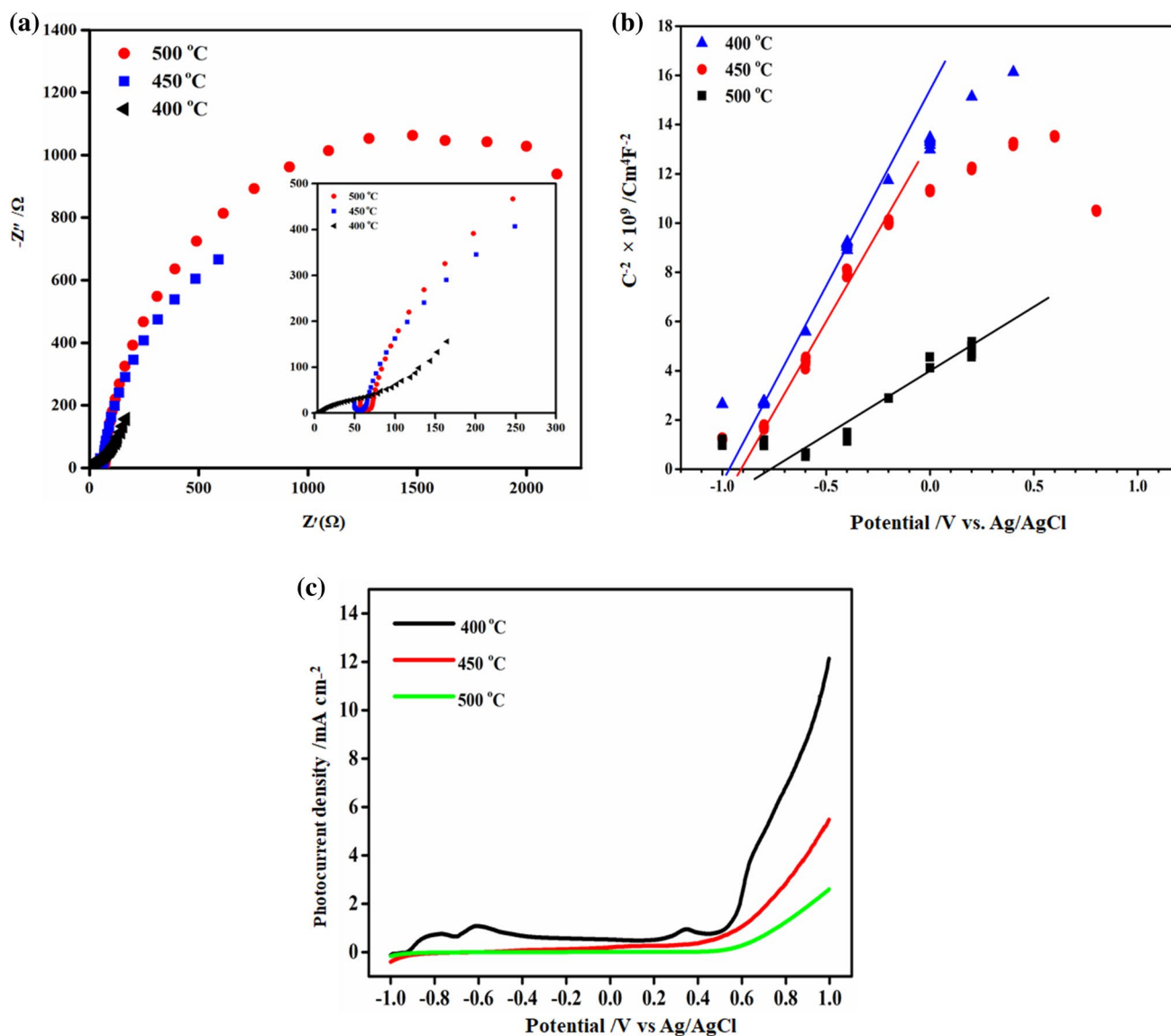


Fig. 2 **a** EIS spectra, **b** M–S plots and **c** I–V curves at different sintering temperatures (thickness: 4L, electrolyte: 1 M KOH and 5 vol%, T: 25 °C)

Table 1 Circuit equivalent fitting data at different sintering temperatures

Sintering temperature (°C)	R_s^a (Ω)	R_{ct} (Ω)	CPE_{SC}^b (F)	n	τ_n^c (ms)	N_D^d (cm ⁻³)	V_{fb}^e (V)
400	4.17	127.18	1.52×10^{-3}	0.6	193.47	2.62×10^{21}	-0.98
450	52.18	1110.2	8.37×10^{-5}	0.99	101	2.2×10^{20}	-0.91
500	58.75	1545.2	6.22×10^{-5}	0.95	96.1	2.91×10^{11}	-0.78

^aResistance

^bConstant phase element

^cElectron lifetime

^dDonor density

^eFlat band potential

400 °C can be explained by the collapse of porous structure and production of some new surface states (mainly from the surface atoms), which can control the electron transfer through the surface state and increase recombination rate [29]. Furthermore, the collected data from M–S plots (Fig. 2b) confirm that donor density was reduced and flat band shifted to a positive potential with the negative influence on the reduction of water to hydrogen [30]. In addition, I–V curves versus applied potential (Fig. 2c) reveals that increasing sintering temperature reduced the photocurrent density on the electrode/electrolyte interface due to high R_{ct} and recombination rate.

3.3 Photoanode thickness

Figure 3 shows the effect of photoanode thickness (number of printed layers; 2L, 3L, 4L, and 5L) on the hydrogen production. Cross section FESM images (Fig. S3) of each photoanode shows thicknesses of 12.25, 18.59, 24.8, and 31.5 μm for 2L, 3L, 4L, and 5L, respectively. The accumulative hydrogen production increased as the photoanode thickness was increased from 2 to 4L. However, the total produced hydrogen reduced up to 5 mL by exceeding the number of printing layers beyond the optimum level. A similar trend was reported by Michael et al. for 4-chlorophenol degradation [31].

EIS spectra (Fig. 4a) and its fitting data (Table 2) confirm that the electron transport resistance decreased when the thin film thickness was increased up to 4L. The R_{ct} value reduced from 2 to 4L because the interfacial adhesion between Cu–Ni/TiO₂ nanoparticles and FTO substrate was enhanced in the alkaline solution [32]. Increasing

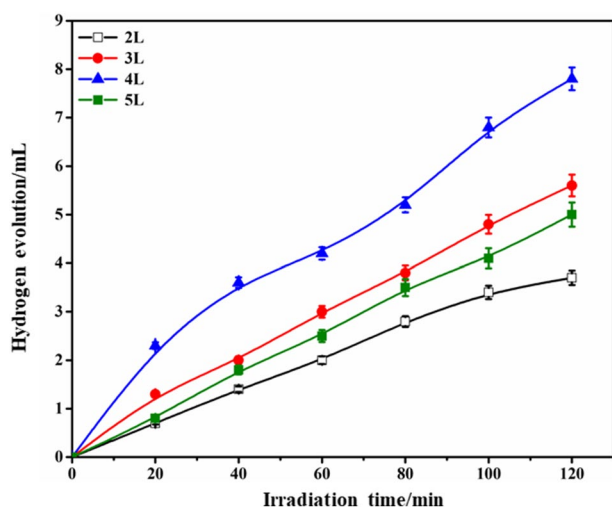


Fig. 3 Effect of different photoanode thicknesses on hydrogen production (thickness: 2–5L, electrolyte: 1 M KOH and 5 vol%, T: 25 °C)

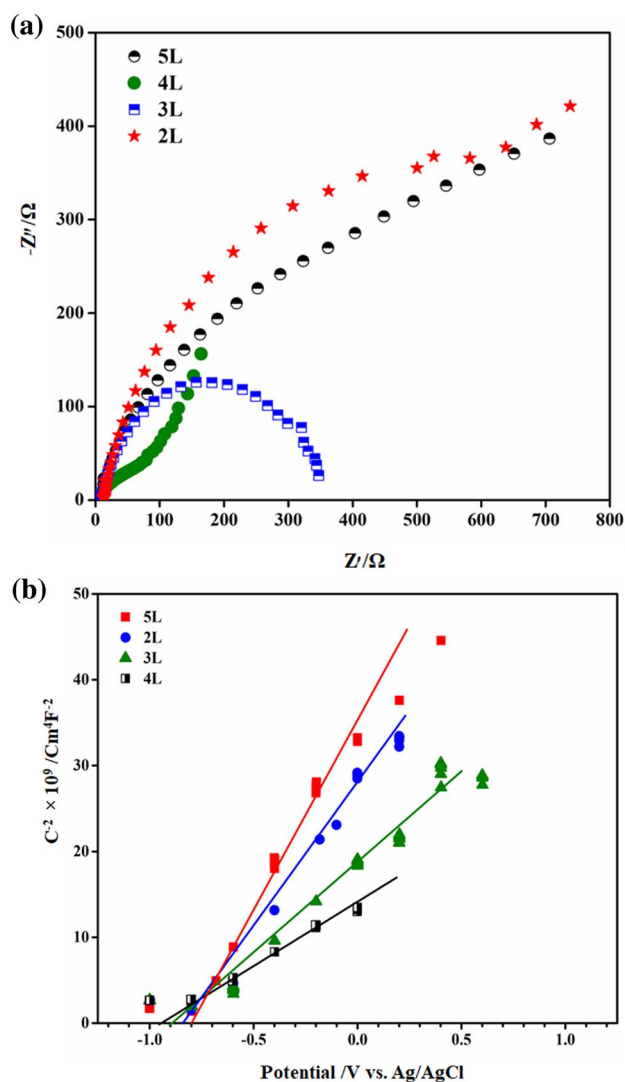
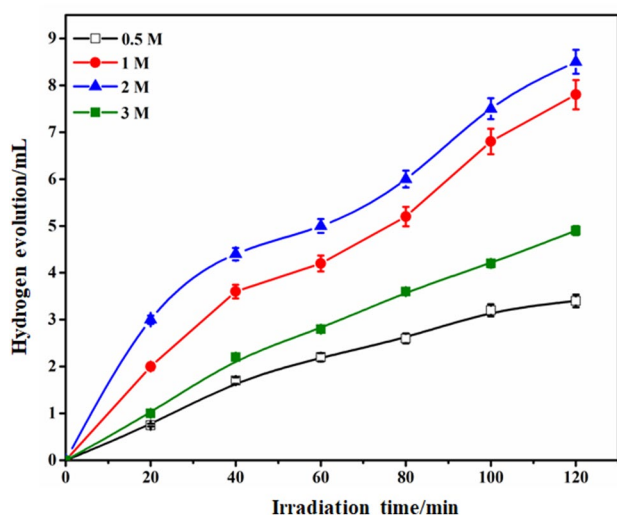


Fig. 4 a EIS spectra and b M–S plots for different photoanode thicknesses (thickness: 2–5L electrolyte: 1 M KOH and 5 vol%, T: 25 °C)

photoanode thickness generated more excited electrons due to better light absorption and more contribution of the Cu–Ni/TiO₂ photocatalyst on the photocatalytic reaction [33]. The R_{ct} increased and the electron lifetime reduced when the photocatalyst layers were beyond the optimum thickness possibly due to the long path for the photogenerated electrons and the high electrolyte penetration in the photoanodes [34–36]. In addition, M–S plots (Fig. 4b) show flat band potentials slightly shifted to a more negative potential by increasing the thickness up to 4L. In addition, increasing donor density by thickness until 4L (Table 2) confirmed the increase in electron transfer from the bulk to the electrode surface and the decrease in resistance at the electrode/electrolyte interface [37].

Table 2 Circuit equivalent fitting results for different photoanode thicknesses

Number of printed layers	R_S^a (Ω)	R_{ct} (Ω)	CPE_{SC}^b (F)	n	τ_n^c (ms)	N_D^d (cm^{-3})	V_{fb}^e (V)
2L	12.6	718	1.19×10^{-4}	0.84	85.12	6.56×10^{20}	-0.82
3L	2.89	332.53	3.55×10^{-4}	0.85	117.97	1.13×10^{21}	-0.95
4L	4.17	127.18	1.52×10^{-3}	0.60	193.47	2.62×10^{21}	-0.9
5L	10.07	536	1.48×10^{-4}	0.90	79.54	5.48×10^{20}	-0.8

^aResistance^bConstant phase element^cElectron lifetime^dDonor density^eFlat band potential**Fig. 5** Influence of different electrolyte concentrations on hydrogen production [thickness: 4L (electrolyte: 0.5–3) M KOH and 5 vol%, T: 25 °C]

3.4 Electrolyte concentration

Electrolyte concentration is another important parameter in PEC cells; it controls the ionic transfer in solution and electrical resistance of electrolytes [38–40]. Normally, high electrolyte concentration can enhance the PEC cell performance up to the optimum level, as shown in Fig. 5. Photocatalytic hydrogen production was increased from 0.5 (3.4 mL) to 2 M (8.5 mL). However, increasing KOH concentration beyond the optimum level (2 M) has a negative effect on hydrogen production.

The concentration of the supporting electrolyte should be sufficiently high (> 0.5 M) to avoid large ohmic voltage losses across the electrolyte. Figure 6a and Table 3 represent the Nyquist spectra and the fitting data of photocatalyst performance at different KOH solutions. The results confirmed that R_{ct} and R_E (intersection of the EIS

spectrum with Z') decreased when the KOH concentration was increased up to 2 M.

However, the photocurrent densities decreased when the KOH concentration exceeding 2 M (Fig. 6b) due to high electrolyte resistance (R_E) and R_{ct} . The increasing R_E results in voltage loss at the system as expected by Eq. (2) [41, 42].

$$V_{\text{loss}} = I \times R_E \quad (2)$$

Furthermore, the M–S plots shown in Fig. 6c demonstrate that the electrolyte concentration can shift the flat band potential to a negative potential until 2 M. However, a slightly positive shift in the flat band potential was observed in the electrolyte with 3 M KOH, which had a negative effect on hydrogen production. The 2 M KOH solution was selected as the optimum electrolyte concentration for further study.

3.5 Applied voltage

Figure 7a reveals solar hydrogen production as a function of applied voltage (0.7, 3.4, 5.5, 9.5, and 16.5 V) under the optimum reaction conditions. The maximum produced hydrogen under optimum conditions over the applied voltage of 0.7 eV was 8.5 mL, whereas the produced hydrogen sharply increased until 24.6 mL at the applied voltage of 3.4 V. Increasing voltage until 16.5 V reduced the hydrogen production to 19.6 mL. The optimum applied voltage of 3.4 V [1.9 V vs. reduced hydrogen electrode (RHE)] agrees with the practical reported voltage between 1.6 and 2 V versus RHE [9]. Improving the photocatalytic performance of system were related to increasing photocurrent density, minimizing the charge carrier recombination and charge transfer resistance in the photoanode up to optimum level [40, 41]. However, increasing the applied potential beyond the optimum level has the negative effect of hydrogen production in which reaction rate remained almost constant by applying more potential. High-applied potential can fully separate photogenerated charge carriers and increase photocurrent saturation on the surface of photoanode, resulting

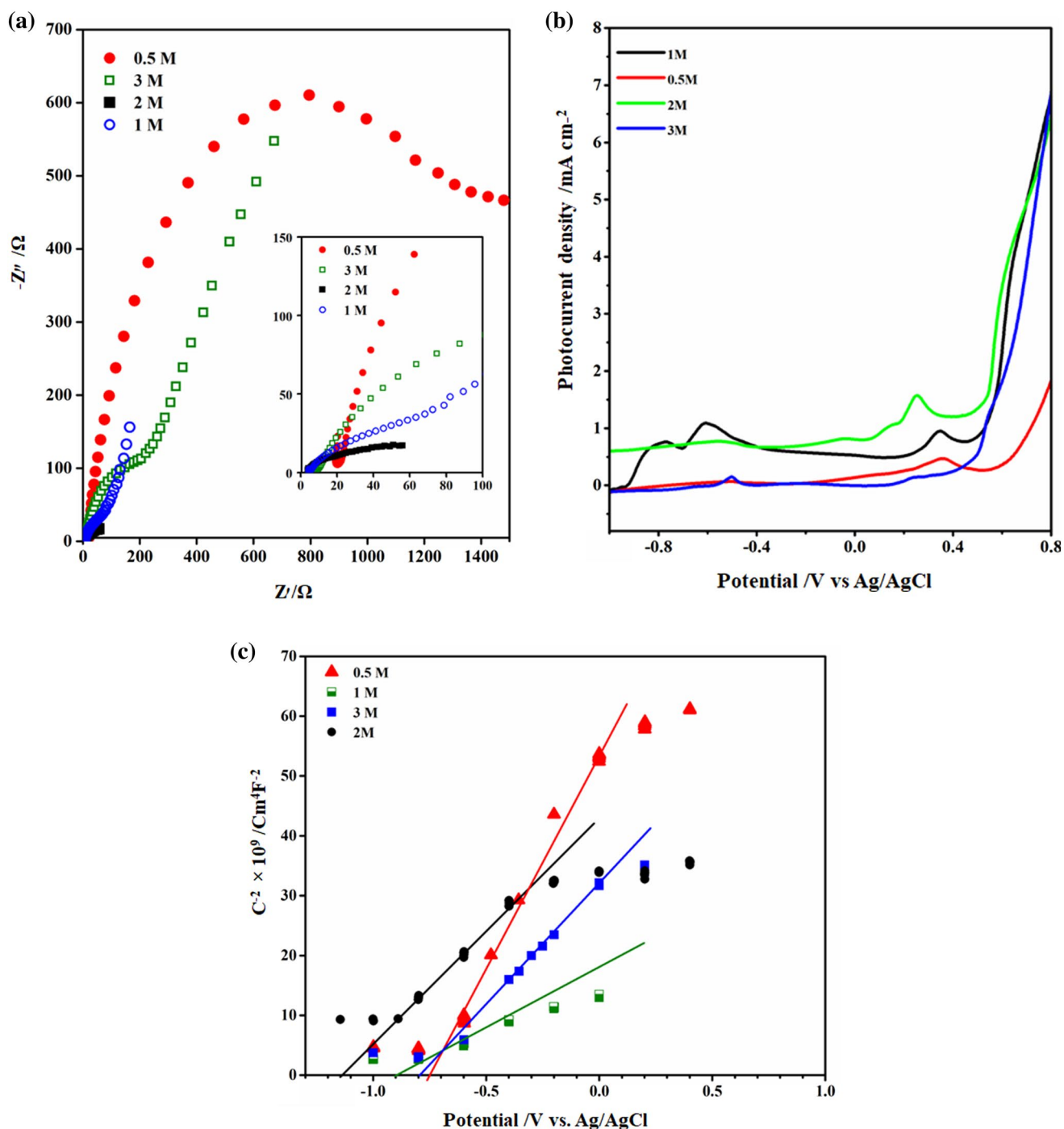


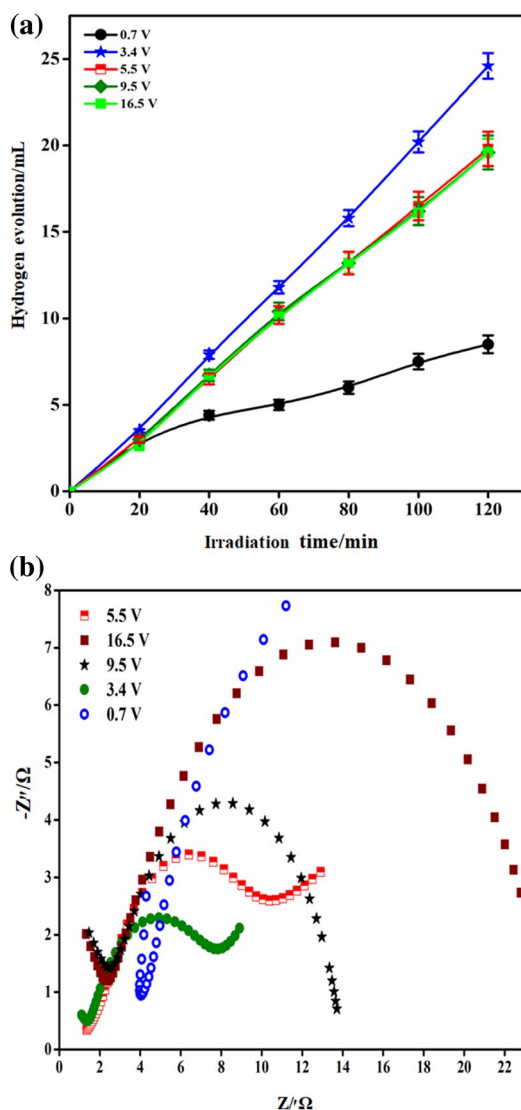
Fig. 6 **a** EIS spectra, **b** I–V curves and **c** M–S plots in different KOH solutions [thickness: 4L (electrolyte: 0.5–3) M KOH and 5 vol%, T: 25 °C]

in high charge transfer resistance and recombination rates as confirmed in EIS spectra (Fig. 7b). The R_{ct} value sharply reduced from 22.45 to 7.45 Ω by increasing voltage from 0.7 to 3.4 V (Table S1) due to improved separation of the photogenerated charge carriers and more photoexcited electrons on the surface of the electrode and the electrolyte, saturating the photocurrent on the surface of the photoanode with the

negative effect on hydrogen production. However, increasing applied voltage from 5.5 to 16.5 V were caused the R_{ct} increased from 6.08 to 22.28 V (Table S1). High-applied voltage causes increasing the number of hydrogen bubbles on the surface of Pt electrode and electrical resistance, diminishing the electron transfer and increasing the ohmic loss of the whole system [38]. The maximum hydrogen

Table 3 Circuit equivalent fitting results with different KOH concentrations

KOH concentration (M)	R_E^a (Ω)	R_{ct} (Ω)	CPE_{sc}^b (F)	n	τ_n^c (ms)	V_{fb}^d (V)
0.5	21	1408.60	3.21×10^{-5}	0.89	45.27	-0.75
1	4.64	127.18	1.52×10^{-3}	0.60	193.47	-0.9
2	4.16	24.45	9.09×10^{-3}	0.96	222	-1.12
3	9	115.44	9.19×10^{-5}	0.94	10.61	-0.8

^aElectrolyte resistance^bConstant phase element^cElectron lifetime^dFlat band potential**Fig. 7** a Hydrogen production and b EIS spectra of different applied voltages [thickness: 4L (electrolyte: 2 M KOH and 5 vol%, T: 25 °C)]

production difference between the highest and lowest levels of applied voltage was 16.5 mL. Thus, this parameter can be considered as the most effective parameter among the applied parameters. However, further optimization of hydrogen production is limited due to its maximum effect around the practical voltage of the PEC cell in the range of 1.6–2 V. We compared the photocatalytic performance of 5 mol% Cu–Ni/TiO₂ photoanode under the optimum conditions with those of photoanodes in relevant past works in PEC/DSSC system. However, the comparison was difficult because different photoanodes and reaction conditions were used. Therefore, data were scaled to a light intensity of 100 mW cm⁻², a geometric area of 1 cm² and an applied voltage of 3.4 V. The scaled data of reported hydrogen production rate by Lee et al. [43] and Shi et al. [7] were 3.35 mL h⁻¹ cm⁻² over WO₃ and 4.72 mL h⁻¹ cm⁻² over WO₃/BiVO₄, respectively in the PEC/DSSC system. The fabricated 5 mol% Cu–Ni/TiO₂ photoanode with a hydrogen production rate of 12.45 mL h⁻¹ cm⁻² can facilitate the transportation of electron to the photoanode/electrolyte interface and enhance PEC/DSSC performance. The better performance of this photocatalyst confirms that CB edges of bulk WO₃ and BiVO₄ are excessively positive for hydrogen production compared with water reduction potential.

3.6 Stability testing of photoanode

The long-term performance of the PEC/DSSC system was tested by immersing the modified 5 mol% Cu–Ni/TiO₂ photoanode with the thickness of 4L in 2 M KOH under the applied voltage of 3.4 V. Figure 8 shows the activity of the optimized photocatalyst during 4 days of illumination from 8 am to 8 pm.

Table 4 shows the volume of produced hydrogen and the photo-voltage of the system for each day with the total accumulative hydrogen production of 443.4 mL. The hydrogen production rate gradually declined from the first to the fourth day, although the system voltage slightly increased at the second and third days. The increase in system voltage may

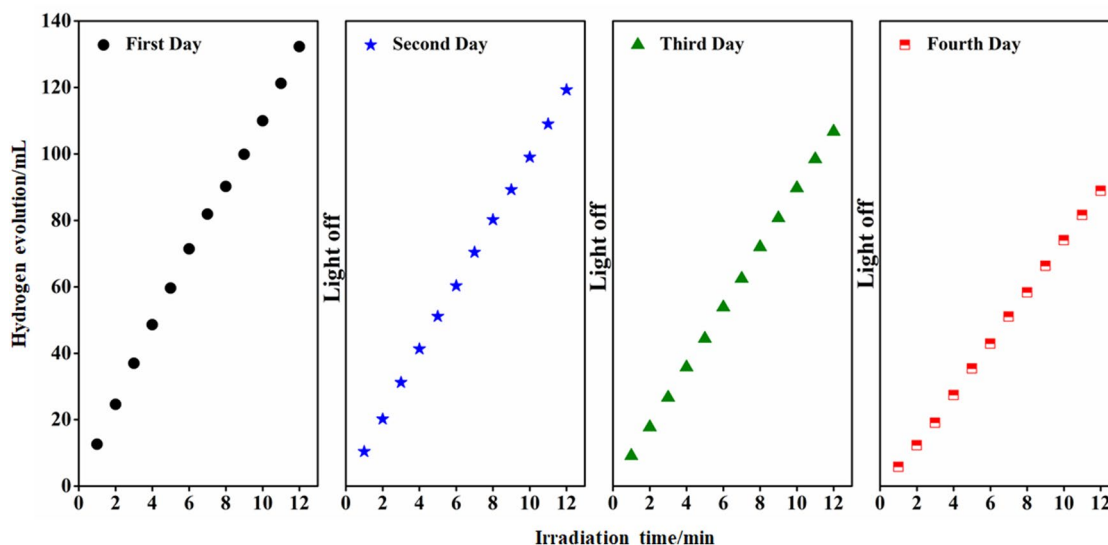


Fig. 8 Trend of hydrogen production for 4 days [thickness: 4L (electrolyte: 2 M KOH and 5 vol%, T: 25 °C)]

be related to the increase in DSSC voltage for long-term irradiation as reported by Xue et al. [44].

The rate of hydrogen production reduced during 4 days in the closed system due to the increase in electrolyte concentration, decrease in the number of H^+ ions in the solution, high resistance on the Pt surface, and reverse reaction between oxygen and hydrogen. Furthermore, the observed oxygen bubbles around the photoanode on the fourth day indicated the reduced amount of glycerol as a sacrificial agent in the solution. Therefore, the slow oxidizing process of OH^- increased the charge carrier recombination rate and decreased the hydrogen production rate.

4 Conclusion

The effect of important experimental parameters on the analytical performance of the PEC/DSSC system was investigated. Optimization process demonstrates that the photoanode thin film fabrication controls the electrochemical properties of photocatalysts, which in turn affects the

photocatalytic activity. Furthermore, no linear trend was observed between hydrogen production and reaction parameters in the PEC/DSSC system. The optimization of the reaction parameters demonstrated that the sintered 5 mol% Cu–Ni/TiO₂ photoanode at 400 °C with the thickness of 4L in 2 M KOH solution under the applied voltage of 3.4 V produced the maximum hydrogen of 24.9 mL. The optimization results confirm that applied voltage exerts the most significant effect on the photocatalytic hydrogen production among the parameters used. Highly stable photocatalyst in the PEC/DSSC system can generate sufficient voltage for photocatalysis to produce 443.4 mL of hydrogen after 4 days. The optimization of the preparation condition for the photoanode and reaction parameters introduce cost-effective and less complex system to improve solar hydrogen production.

Table 4 Total hydrogen production volume, rate and photo-voltage for 4 days

Duration	Hydrogen production		Recorded voltage in system	
	Volume (mL)	Rate (mL h ⁻¹)	$V_{Ag/AgCl}$	V_{RHE}
First day	132.3	10.98	0.89	1.88
Second day	119.3	9.9	0.952	1.94
Third day	102.9	8.58	1.06	2.05
Forth day	88.9	7.39	1.08	2.06

Acknowledgements The authors would like to thank Universiti Teknologi PETRONAS and Centre of Innovative Nanostructures & Nanodevices (COINN) for technical support to make this research work feasible.

References

- Leung DYC, Fu X, Wang C, Ni M, Leung MKH, Wang X et al (2010) Hydrogen production over titania-based photocatalysts. *ChemSusChem* 3(6):681–694
- Zhu J, Zäch M (2009) Nanostructured materials for photocatalytic hydrogen production. *Curr Opin Colloid Interface Sci* 14(4):260–269
- Gan J, Lu X, Tong Y (2014) Towards highly efficient photoanodes: boosting sunlight-driven semiconductor nanomaterials for water oxidation. *Nanoscale* 6(13):7142–7164
- Tüysüz H, Chan CK (2013) Preparation of amorphous and nanocrystalline sodium tantalum oxide photocatalysts with porous matrix structure for overall water splitting. *Nano Energy* 2(1):116–123
- Fujishima A, Honda K (1972) Electrochemical photolysis of water at a semiconductor electrode. *Nature* 238(5358):37–38
- Stratiki N, Bekiari V, Kondarides DI, Lianos P (2007) Hydrogen production by photocatalytic alcohol reforming employing highly efficient nanocrystalline titania films. *Appl Catal B* 77:184–189
- Shi X, Zhang K, Shin K, Ma M, Kwon J, Choi IT et al (2015) Unassisted photoelectrochemical water splitting beyond 5.7% solar-to-hydrogen conversion efficiency by a wireless monolithic photoanode/dye-sensitized solar cell tandem device. *Nano Energy* 13:182–191
- Bak T, Nowotny J, Rekas M, Sorrell CC (2002) Photo-electrochemical hydrogen generation from water using solar energy. Materials-related aspects. *Int J Hydrogen Energy* 27(10):991–1022
- Minggu LJ, Wan Daud WR, Kassim MB (2010) An overview of photocells and photoreactors for photoelectrochemical water splitting. *Int J Hydrogen Energy* 35(11):5233–5244
- Grätzel M (2003) Dye-sensitized solar cells. *J Photochem Photobiol C* 4(2):145–153
- Son M-K, Seo H, Kim S-K, Hong N-Y, Kim B-M, Park S et al (2013) Improved long-term durability of a parallel-type dye-sensitized solar cell module using a platinum metal grid fabricated by direct current magnetron sputtering with heat treatment. *J Power Sources* 222:333–339
- Grätzel M (1999) The artificial leaf, bio-mimetic photocatalysis. *Cattech* 3:3–17
- Townsend TK, Sabio EM, Browning ND, Osterloh FE (2011) Photocatalytic water oxidation with suspended alpha-Fe₂O₃ particles—effects of nanoscaling. *Energy Environ Sci* 4(10):4270–4275
- Moniz SJA, Shevlin SA, Martin DJ, Guo Z-X, Tang J (2015) Visible-light driven heterojunction photocatalysts for water splitting—a critical review. *Energy Environ Sci* 8(3):731–759
- Lu X, Xie S, Yang H, Tong Y, Ji H (2014) Photoelectrochemical hydrogen production from biomass derivatives and water. *Chem Soc Rev* 43(22):7581–7593
- Colon G, Maicu M, Hidalgo M, Navio J (2006) Cu-doped TiO₂ systems with improved photocatalytic activity. *Appl Catal B* 67(1–2):41–51
- Sun T, Fan J, Liu E, Liu L, Wang Y, Dai H et al (2012) Fe and Ni co-doped TiO₂ nanoparticles prepared by alcohol-thermal method: application in hydrogen evolution by water splitting under visible light irradiation. *Powder Technol* 228:210–218
- Pelaez M, Nolan NT, Pillai SC, Seery MK, Falaras P, Kontos AG et al (2012) A review on the visible light active titanium dioxide photocatalysts for environmental applications. *Appl Catal B* 125:331–349
- Shiraishi Y, Sakamoto H, Sugano Y, Ichikawa S, Hirai T (2013) Pt–Cu bimetallic alloy nanoparticles supported on anatase TiO₂: highly active catalysts for aerobic oxidation driven by visible light. *ACS Nano* 7(10):9287–9297
- Gallo A, Marelli M, Psaro R, Gombac V, Montini T, Fornasiero P et al (2012) Bimetallic Au-Pt/TiO₂ photocatalysts active under UV-A and simulated sunlight for H₂ production from ethanol. *Green Chem* 14(2):330–333
- Bashiri R, Mohamed NM, Fai Kait C, Sufian S, Khatani M (2017) Enhanced hydrogen production over incorporated Cu and Ni into titania photocatalyst in glycerol-based photoelectrochemical cell: effect of total metal loading and calcination temperature. *Int J Hydrogen Energy* 42(15):9553–9566
- Bashiri R, Mohamed NM, Fai Kait C, Sufian S, Kakooei S, Khatani M et al (2016) Optimization hydrogen production over visible light-driven titania-supported bimetallic photocatalyst from water photosplitting in tandem photoelectrochemical cell. *Renew Energy* 99:960–970
- Mohamed NM, Bashiri R, Fai Kait C, Sufian S, Kakooei S (2015) Photoelectrochemical behavior of bimetallic Cu–Ni and monometallic Cu, Ni doped TiO₂ for hydrogen production. *Int J Hydrogen Energy* 40(40):14031–14038
- Fattah-alhosseini A, Torkaman M, Karami E (2015) Electrochemical and semiconducting behaviour of a brass alloy in borax solutions. *J Mater Environ Sci* 6(3):885–891
- Lekse JW, Haycock BJ, Lewis JP, Kauffman DR, Matranga C (2014) The effect of electronic structure changes in NaInO₂ and NaIn_{0.9}Fe_{0.1}O₂ on the photoreduction of methylene blue. *J Mater Chem A* 2(24):9331–9337
- Palmas S, Polcaro AM, Ruiz JR, Da Pozzo A, Mascia M, Vacca A (2010) TiO₂ photoanodes for electrically enhanced water splitting. *Int J Hydrogen Energy* 35(13):6561–6570
- Boschloo GK, Goossens A, Schoonman J (1997) Photoelectrochemical study of thin anatase TiO₂ films prepared by metalorganic chemical vapor deposition. *J Electrochem Soc* 144(4):1311–1317
- Zhao D, Peng T, Lu L, Cai P, Jiang P, Bian Z (2008) Effect of annealing temperature on the photoelectrochemical properties of dye-sensitized solar cells made with mesoporous TiO₂ nanoparticles. *J Phys Chem C* 112(22):8486–8494
- Lu L, Li R, Fan K, Peng T (2010) Effects of annealing conditions on the photoelectrochemical properties of dye-sensitized solar cells made with ZnO nanoparticles. *Sol Energy* 84(5):844–853
- Liu Q, Ding D, Ning C, Wang X (2015) Black Ni-doped TiO₂ photoanodes for high-efficiency photoelectrochemical water-splitting. *Int J Hydrogen Energy* 40(5):2107–2114
- Hitchman LM, Tian F (2002) Studies of TiO₂ thin films prepared by chemical vapour deposition for photocatalytic and photoelectrocatalytic degradation of 4-chlorophenol. *J Electroanal Chem* 538–539:165–172
- Zhang H, Wang W, Liu H, Wang R, Chen Y, Wang Z (2014) Effects of TiO₂ film thickness on photovoltaic properties of dye-sensitized solar cell and its enhanced performance by graphene combination. *Mater Res Bull* 49:126–131
- Song X-M, Wu J-M, Yan M (2008) Photocatalytic and photoelectrocatalytic degradation of aqueous Rhodamine B by low-temperature deposited anatase thin films. *Mater Chem Phys* 112(2):510–515
- Bennani Y, Appel P, Rietveld LC (2015) Optimisation of parameters in a solar light-induced photoelectrocatalytic process with a TiO₂/Ti composite electrode prepared by paint-thermal decomposition. *J Photochem Photobiol A* 305:83–92

35. Lopes T, Andrade L, Ribeiro HA, Mendes A (2010) Characterization of photoelectrochemical cells for water splitting by electrochemical impedance spectroscopy. *Int J Hydrogen Energy* 35(20):11601–11608
36. Andrade L, Cruz R, Ribeiro HA, Mendes A (2010) Impedance characterization of dye-sensitized solar cells in a tandem arrangement for hydrogen production by water splitting. *Int J Hydrogen Energy* 35(17):8876–8883
37. Chiang C-Y, Aroh K, Dass S, Ehrman S, Franson N, Satsangi VR (2011) Copper oxide nanoparticle made by flame spray pyrolysis for photoelectrochemical water splitting—part II. Photoelectrochemical study. *Int J Hydrogen Energy* 36(24):5519–5526
38. Zeng K, Zhang D (2010) Recent progress in alkaline water electrolysis for hydrogen production and applications. *Prog Energy Combust Sci* 36(3):307–326
39. Ren K, Gan YX, Nikolaidis E, Sofyani SA, Zhang L (2013) Electrolyte concentration effect of a photoelectrochemical cell consisting of nanotube anode. *Mater Sci* 2013:1–7
40. Zhang S, Zhao H, Jiang D, John R (2004) Photoelectrochemical determination of chemical oxygen demand based on an exhaustive degradation model in a thin-layer cell. *Anal Chim Acta* 514(1):89–97
41. Yuvaraj AL, Santhanaraj D (2014) A systematic study on electrolytic production of hydrogen gas by using graphite as electrode. *Int Sch Res Notices* 17(1):83–87
42. Mahrous A, Sakr I, Balabel A, Ibrahim K (2011) Experimental investigation of the operating parameters affecting hydrogen production process through alkaline water electrolysis. *IJTEE* 2(2):113–116
43. Lee WJ, Shinde PS, Go GH, Ramasamy E (2011) Ag grid induced photocurrent enhancement in WO_3 photoanodes and their scale-up performance toward photoelectrochemical H_2 generation. *Int J Hydrogen Energy* 36(9):5262–5270
44. Xue G, Guo Y, Yu T, Guan J, Yu X, Zhang J et al (2012) Degradation mechanisms investigation for long-term thermal stability of dye-sensitized solar cells. *Int J Electrochem Sci* 7:1496–1511